Materials Advances

ROYAL SOCIETY OF CHEMISTRY

PAPER

View Article Online
View Journal | View Issue

Cite this: *Mater. Adv.*, 2022, 3, 2070

Emissive organogel mediated construction of a flexible covalent organic polymer for the separation of aniline for water purification†

Sayan Maiti, Tapas Ghosh, Arati Samal and Apurba K. Das *

Received 16th December 2021,
Accepted 29th December 2021

DOI: 10.1039/d1ma01190a

rsc.li/materials-advances

A flexible covalent organic polymer (**COP**) has been successfully synthesized *via* dynamic covalent gel (DCG) formation through an imine condensation reaction between 6-hydrazinonicotinic hydrazide hydrate and benzene-1,3,5-tricarboxaldehyde within 7 min under ambient conditions. An emissive organogel mediated protocol has been developed for the construction of an amorphous polymer (**COP**), selectively in *N*,*N*-dimethyl acetamide (DMA). Interestingly, two non-emissive building block units without large π-conjugated structures have been engaged for the construction of green emissive **COP-gel**. The green emission of **COP-gel** is generated by the intermolecular H-bonding assisted aggregation induced emission phenomenon. The dried **COP** efficiently adsorbs aniline molecules into its cavities and separates them from binary mixtures of aniline/nitrobenzene and aniline/water, respectively.

Introduction

Covalent organic polymers (COPs) are a unique class of organic porous materials that are constructed covalently from organic subunits.[1] Mostly, COPs are constructed from functional organic building blocks through the formation of B–N, B–O, C═N, C═C, C–N, C═N, C═N/C–O, N═N, and Si–O bonds.[2,3] Several methods or templates have been developed to synthesize COPs.[4–6] However, it is still a difficult task to develop a synthetic approach for the synthesis of large-scale COPs under ambient conditions. In order to extend the implementation of porous organic polymers, a time-efficient synthetic method is being sought. An aggregation assisted synthetic procedure can be the easiest and alternative route for the scalable synthesis of COPs. Covalent dynamic gel formation can be an intermediate aggregated state that can be used for the large scale synthesis of COPs. On the other hand, it is a challenging task to evaluate the nature of covalent dynamic gels despite their various applications in catalysis, sensors and adsorbent materials.[7–10]

Recently, covalent organic polymers (COPs)[11,12] have received considerable importance in membrane technologies due to their selective molecular adsorption and separation properties.[13–18] The characteristics of COPs can be altered at the atomic level by modifying the synthetic procedures and suitable monomers. Functionalized Schiff base covalent organic polymers as membrane materials exhibit high efficiency in the separation of molecules/ions.[19–23] In this regard, the introduction of various functional groups into porous materials has been reported as an effective way to improve their adsorption capacity and selectivity towards organic molecules. The efficient separation of aromatic organic solvents from solvent mixtures and their derivatives, which are critical components of the chemical industry, can lead to higher reusability.

An organic solvent like aniline is a crucial intermediate in the production of medicines, rubber accelerators and anti-aging chemicals.[24] Moreover, aniline is a common organic contaminant with high toxicity, rapid bio-enrichment and challenging biodegradability.[25] Since aniline poses potential danger in industrial scale separation, and threat to human health and the environment due to its high toxicity, volatility or flammability, there is a strong demand for the development of highly effective and environmentally safe materials for the separation of aniline from solvent mixtures.[26,27] A wide range of methods and technologies have been developed to remove aniline.[28,29] On the other hand, several nitrogen atoms containing recyclable green switchable solvents are widely used for the extraction or separation of organic solvents.[30,31] However, most of the switchable solvents are amines that separate the desired product from the solvent mixtures through a phase transition process. Li *et al.* used nitrogen containing ionic liquids for the separation of binary mixtures by extractive distillation methods.[32] The extractive distillation method can also be used to separate organic solvent mixtures.[33,34] The above-mentioned methods or processes are quite complicated and are characterized by high energy consumption and high equipment cost, therefore, it is necessary to develop a convenient method and

Department of Chemistry, Indian Institute of Technology Indore, Khandwa Road, Indore 453552, India. E-mail: apurba.das@iiti.ac.in

† Electronic supplementary information (ESI) available. See DOI: 10.1039/d1ma01190a

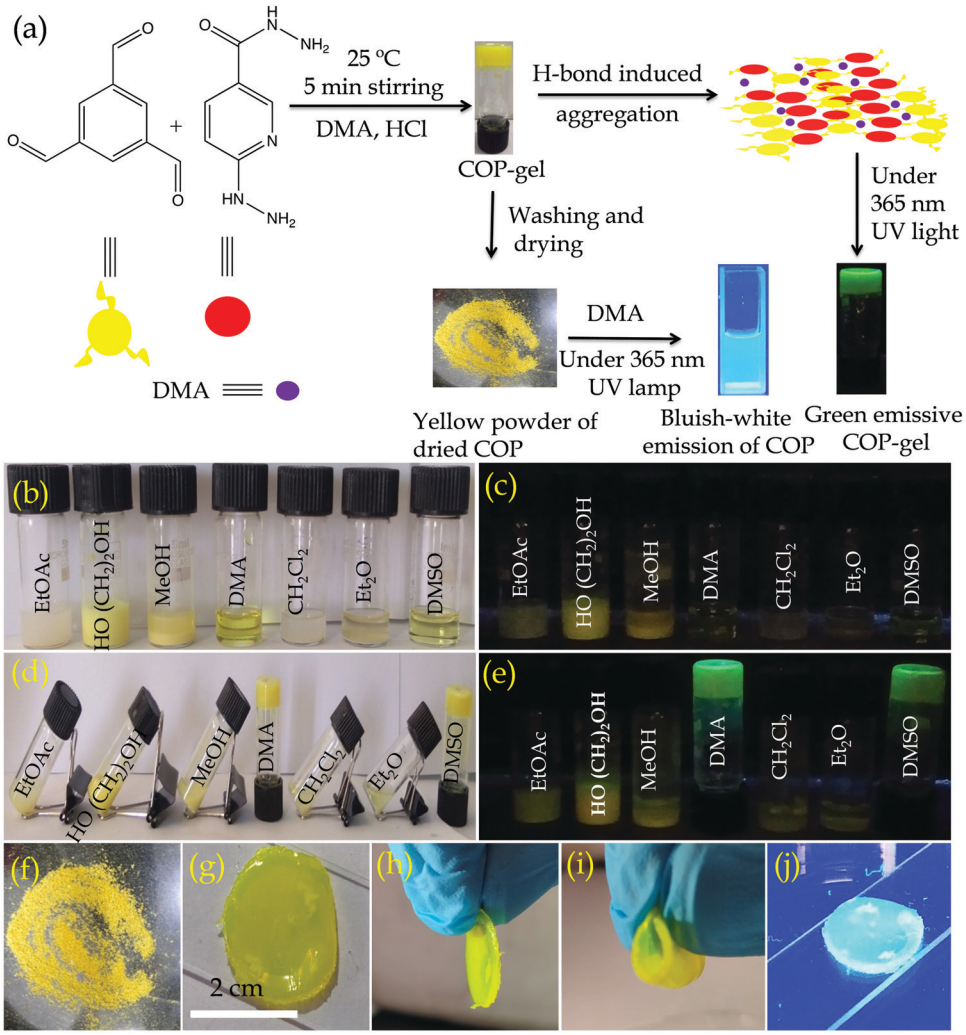

Fig. 1 (a) Schematic representation of porous **COP** synthesis, and aniline separation and adsorption by **COP**. Solution mixture of 6-hydrazinonicotinic hydrazide hydrate and benzene-1,3,5-tricarboxaldehyde in different solvents (b) in day light and (c) under 365 nm UV light. Solution mixture of 6-hydrazinonicotinic hydrazide hydrate and benzene-1,3,5-tricarboxaldehyde in different solvents after the addition of 1N HCl (d) in day light and (e) under 365 nm UV light. Optical images of (f) **COP** powder, (g–j) films formed with **COP** and (i) **COP** film (shows white-cyan colour emission) under 365 nm UV light.

material with lower equipment costs for the separation of organic solvents. In this regard, adsorption using solid adsorbents is a quick and easy method, and nitrogen functionalized COPs can be innovative solid adsorbent materials with high adsorption capacity and selectivity for the separation of organic solvents. The adsorption technique is demonstrated to be enhanced with better adsorption capacity and selectivity due to the possible H-bonding, and electrostatic and acid–base interactions between the surface functional groups on the COPs and adsorbates. Herein, our objectives are (1) to develop new synthetic methodologies with large-scale synthesis of functionalized COP materials under ambient conditions, (2) to develop cavities inside the COP backbone through the dynamic covalent gel (DCG) strategy and (3) to investigate the intrinsic properties of functionalized COP materials. In this work, we have synthesized hydrazine, hydrazide and pyridine group functionalized **COP** *via* emissive organogel formation within 7 min (Fig. 1a). The gel formation plays a key role in synthesizing the **COP** on a large scale. The **COP** is capable of adsorbing or encapsulating aniline selectively in its cavities and selectively separates it from binary mixtures of aniline/nitrobenzene and aniline/water.

Results and discussion

Here we have developed a facile synthetic strategy to synthesize covalent organic polymers with 6-hydrazinonicotinic hydrazide hydrate and benzene-1,3,5-tricarboxaldehyde as building block units. The **COP** has been synthesized *via* emissive organogel formation in DMA under acidic conditions within 7 min (Fig. 1a) under ambient conditions. The gel is formed with a **COP** concentration of about 0.038–0.040 mol L^{-1}. Among ethyl acetate (EtOAc), diethyl ether (Et_2O), ethylene glycol $(CH_2OH)_2$, methanol (MeOH), *N*,*N*-dimethyl acetamide (DMA), dichloromethane (CH_2Cl_2) and

dimethyl sulfoxide (DMSO), the **COP** was successfully formed in DMA *via* emissive gel formation (Fig. 1). Fig. S1 (ESI†) shows the 3D block representation of **COP-gel**. To obtain pure **COP**, the **COP-gel** was dried and washed several times with water, ethyl acetate, *N*,*N*-dimethyl formamide, and methanol to remove unusual impurities. After drying at 90 °C, the **COP** was characterized using several techniques.

The FT-IR spectrum of **COP** demonstrates the successful construction of **COP** *via* the formation of –C═N bonds.[35–37] The peaks at 1530 and 1605 cm^{-1} are assigned to –C═C– and –C═N bond stretching. A peak at 1650 cm^{-1} appears due to the –C(═O)NHNH– stretching band (Fig. 2a). The powder XRD pattern of **COP** suggests that the polymer is successfully constructed from two crystalline secondary building block units (Fig. 2b). The broad powder XRD pattern of **COP** exhibits its amorphous polymeric nature (Fig. 2b). A slight broad peak at higher 2θ indicates the strong π–π stacking interaction between the **COP** layers. To investigate the thermal stability of **COP**, we have performed thermogravimetric analysis (Fig. 3a). The **COP** exhibits high thermal stability. The TGA spectrum of **COP** shows a 4% weight loss in the lower temperature range from 27 to 230 °C due to the evaporation of adsorbed moisture in **COP**, followed by weight losses of around 6.34% and 15.95% over the temperature range of 230 to 370 °C and 370 to 402 °C, respectively. Following that, a gradual loss of weight is observed as the temperature increases.

The solid-state ^{13}C CP-MAS NMR spectrum of **COP** also supports the successful formation of **COP** (Fig. 3b). The peaks from 120–140 ppm confirm the presence of phenyl groups. The peak at 159 ppm suggests acyl hydrazone groups in **COP**. The peak at 163 ppm confirms the presence of carbonyl groups of –C(O)NHNH– and a peak at 150 ppm appears due to the C═N bond of the pyridine ring.[35]

The porosity of **COP** was evaluated by performing BET surface area analysis by N_2 sorption at 77 K and 1 bar pressure. No hysteresis loop is observed in the isotherm. The **COP** shows a type II reversible isotherm (Fig. S2, ESI†). The presence of micropores is demonstrated by a steep uptake at a low relative pressure P/P_0. This result clearly suggests that microporosity has been observed inside the **COP** during the gel formation. At high relative pressures of $P/P_0 > 0.9$, a significant volume of N_2 adsorption is observed. The increase in N_2 adsorption at $P/P_0 > 0.9$ and the complete absence of saturation in the adsorption isotherm can be ascribed to the condensation of N_2 gas molecules in inter-particular voids or in larger pores. The calculated BET surface area of **COP** is 49.69 $m^2\ g^{-1}$. The pore size distribution of **COP** was studied *via* the NLDFT method (Fig. S3, ESI†). The calculated pore volume of **COP** is 0.49 cc g^{-1}. The rheology of **COP-gel** was determined at ambient temperature to evaluate the mechanical properties of **COP-gel** (Fig. 3c and d). The oscillatory frequency sweep test was performed in the frequency range of 0.05 to 100 rad s^{-1} at an applied strain of 1%. The storage modulus (G') is significantly higher than the loss modulus (G'') over the studied frequency range which clearly indicates the viscoelastic and robustness nature of **COP-gel**. According to scanning (SEM) and high resolution transmission electron microscopy (HRTEM) images, **COP** generates a sponge-like porous structure made up of interconnected nanoscale spherical particles (Fig. 4a and b). The particles with a diameter of 20–40 nm combine to form a three-dimensional gel matrix. The amorphous nature of **COP** is also supported by its selected area diffraction pattern (SAED) pattern (Fig. 4b, inset). The surface hydrophobicity and surface roughness of **COP** were evaluated using atomic force microscopy (Fig. 4c). The nano-level surface roughness illustrates the hydrophobicity of **COP**. In general, highly hydrophobic materials have a tendency to aggregate into spherical assembly upon coating on a glass surface.[38] Similarly, the **COP** also shows this salient feature. The **COP** surface contains several crests and troughs which have been observed from the 3D view (Fig. 4d). The peaks in the region of 0.5 μm indicate the existence of air pockets between the peaks (valley regions). These trapped air pockets in the valley region create the hydrophobic pores in **COP**.

The **COP-gel** shows green emission within the range of 520–550 nm. Interestingly two secondary building block units

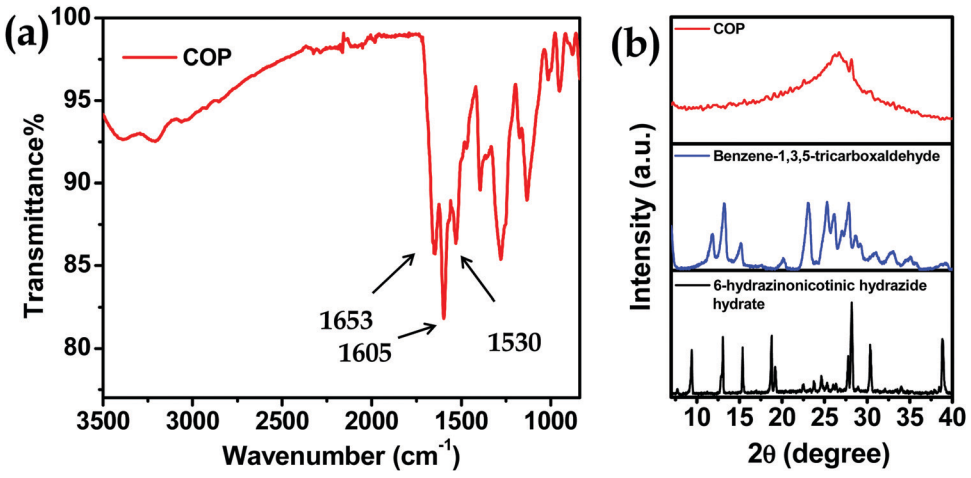

Fig. 2 (a) FT-IR spectrum of **COP**. (b) Powder XRD pattern of **COP**.

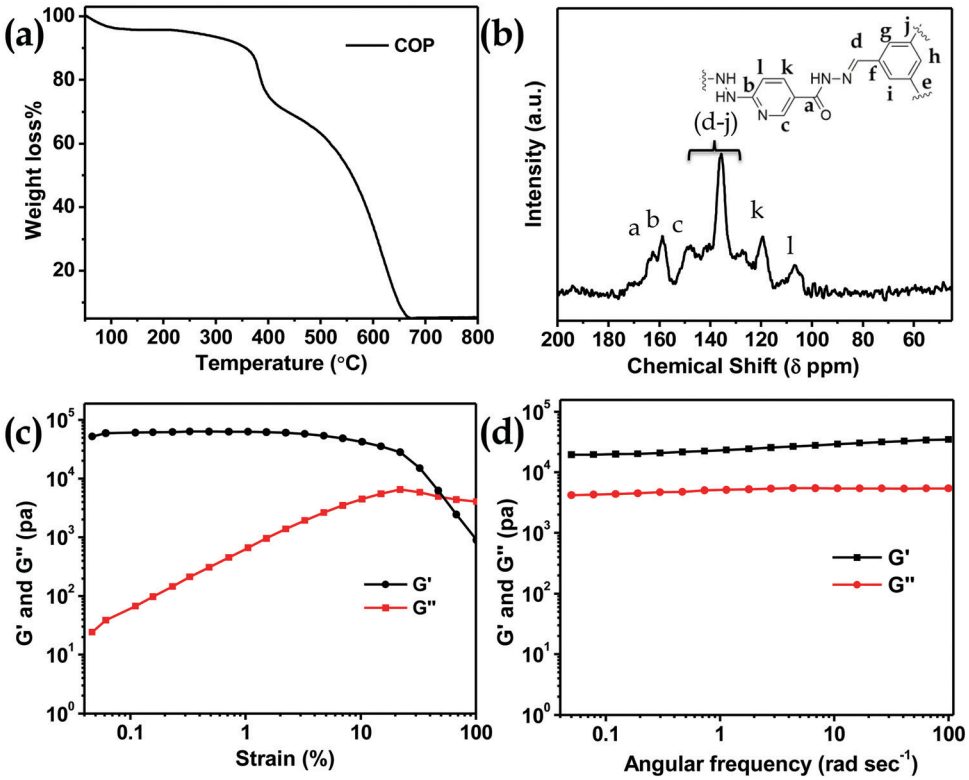

Fig. 3 (a) TGA curve of **COP**. (b) Solid state ^{13}C NMR spectrum of **COP**. Linear viscoelastic (LVE) properties of (c) **COP-gel** and (d) the dynamic frequency sweep experiment of **COP-gel**.

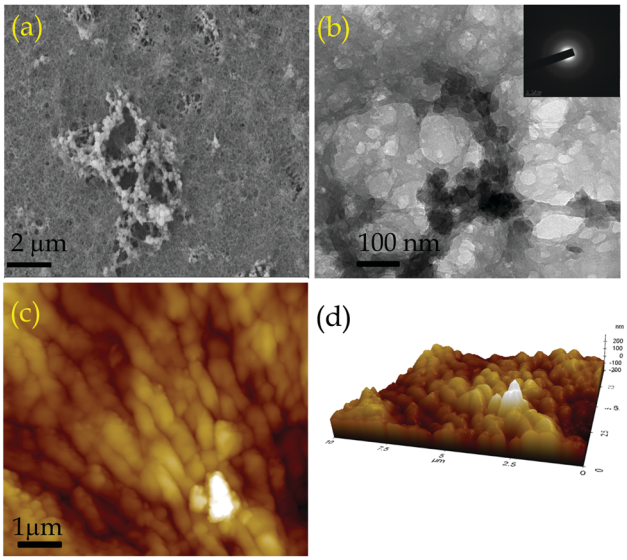

Fig. 4 (a) SEM and (b) HRTEM images of **COP** (Inset: SAED pattern of **COP**). (c) AFM image of **COP** and (d) 3D AFM (*Z*-axis interpretation) image of **COP**.

are non-fluorescent in the DMA solvent and the pyridine moiety is itself a fluorescence quencher. The **COP** backbone is rigidified through a series of H-bonding interaction between the hydrazide groups and the solvent molecule (DMA) (Fig. S4, ESI†). These H-bonds are highly responsible for the restriction of intramolecular rotation, which causes aggregation-induced emission (AIE).[39,40] The emission colour of **COP** originates from the distinct level of aggregation in the solvent which alters the electronic distribution and shows different fluorescent colours. So, H-bonding plays a significant role in the evolution of emissive **COP-gel**. By varying the concentration of building block units, we have also prepared **COP** through flexible thin film preparation in the DMA solvent. Different extents of aggregation occur in gel and thin films, leading to different emission colours (Fig. 1g and j). We have conducted a spectroscopic study in detail to prove that the H-bonding induced strong aggregation in **COP-gel**. The UV-vis spectrum of **COP-gel** shows an absorption maximum centered at 311 nm, which is attributed to the n–π* transition (Fig. S5, ESI†). On the other hand, an absorption peak at 423 nm of **COP-gel** is observed, which suggests the formation of strong intermolecular H-bonds. This phenomenon indicates its higher order aggregated state by restricting intramolecular rotation (RIR) and lowering the HOMO–LUMO energy gap.[41,42] Also, a broader absorption band reveals a higher order aggregated form of **COP-gel** (Fig. S5, ESI†). The **COP-gel** shows dual emission at 530 nm with a shoulder peak at 626 nm (Fig. S6, ESI†). We have also performed temperature dependent fluorescence studies of **COP-gel**. The temperature-dependent fluorescence studies reveal that the emission intensity decreases gradually with the increase in temperature (Fig. S7, ESI†). These results also

support the existence of H-bonding inside the **COP-gel**. The excitation spectrum of **COP-gel** at 530 nm is similar to the excitation spectrum of **COP-gel** at 626 nm (Fig. S8, ESI†). These results indicate that the origin of the shoulder band at around 626 nm of **COP-gel** is assigned to the protonated state.[43] An emission peak at 626 nm originates from the protonated form of the **COP-gel** (due to formation of PyH^+ and imine –C═NH^+–). The green colour emission of **COP-gel** is also visualized under a confocal microscope with an excitation wavelength of 405 nm and emission collection of 540 nm, respectively. The confocal image of **COP** is shown in Fig. S9 (ESI†). The confocal images further support the AIE phenomenon in the solid state of **COP** in the green colour region.[44] We have further investigated the photophysical properties of disperse solutions of **COP** powder in DMA solution. As previously stated, the introduction of hydrazide functionality is crucial for strengthening the COP's emissive behaviour *via* strong intra- and interlayer H-bonding interactions. In the UV-vis spectra of **COP** solution, a broad absorption maximum is found across the wavelength range of 300 to 400 nm, which correlates with the n–π* transitions and also reveals its aggregated state (Fig. S10, ESI†). For an excitation wavelength of 340 nm, the emission spectrum of **COP** in DMA shows a maximum at 474 nm (Fig. S10, ESI†). Pyridine and hydrazide functionalized **COP** showcased adequate thermal and chemical stability due to the presence of several heteroatoms in the polymeric backbone, and H-bonding controlled fluorescence properties in DMA solution. The abundant heteroatoms form intra- and intermolecular H-bonds, causing aggregation, limiting intermolecular rotation, and emitting light. The emission of **COP** in DMA solution is clearly attributed to the intermolecular and intermolecular H-bonding assisted aggregation induced emission properties.

The solvent extraction method is widely used to isolate aromatic organic solvent mixtures and their derivatives. The choice of material is highly influenced by its similarity to the target product, cost and safety. Nitrogen-rich switchable materials, a class of recyclable green materials, can be used to separate the organic solvent mixtures efficiently in a cost-effective manner.[45] Herein, the **COP** acts as an efficient stationary phase for the separation of organic solvents from binary organic solvent mixtures (Fig. 5 and Fig. S11, ESI†).

We have taken aniline/nitrobenzene as a model organic solvent mixture for the separation experiment using dried **COP**. Initially, we loaded 60 mg of **COP** inside a 1 mL (5.5 cm) glass syringe and the packing length was 0.15 mL (0.7 cm). At first, we took 50 μL of each solvent and diluted it with hexane and passed through the **COP** loaded in the 1 mL glass syringe. The **COP** selectively adsorbs and separates aniline from nitrobenzene. Hexane was used as the mobile phase solvent. All the filtrates were characterized by high performance liquid chromatography (HPLC) (Fig. S12 and S13, ESI†). Generally, separation of organic solvents depends on the surface charge of the **COP**, pore size, functionality on the **COP** surface and electrostatic interactions between **COP** and organic solvents. Here, the **COP** exhibits a hydrazide and pyridinic group rich surface with an average pore size distribution of 1.3 to 10 nm.[45–47] Aniline shows high binding interactions and easily stack with the **COP** backbone through –NH···N– interactions that also induce the aggregation properties of **COP** and reside in the pore cavity of the polymer.[48–51] Nitrobenzene, on the

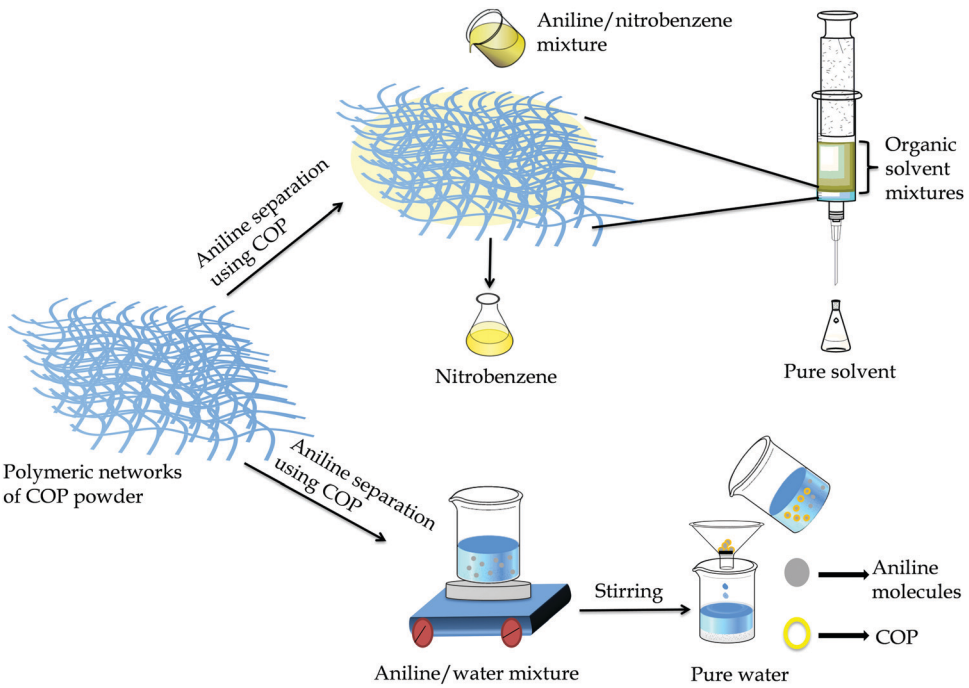

Fig. 5 Schematic representation of aniline separation from binary solvent mixtures aniline/nitrobenzene and aniline/water.

other hand, lacks any polar amine ($-NH_2$) group and is unable to bind with the **COP** backbone. As a result, nitrobenzene can easily escape *via* the **COP**. Hexane (6 mL) is required to remove the entire amount of nitrobenzene. We have also investigated the adsorption limit of aniline using 60 mg **COP** powder. The high adsorption limit of **COP** is found to be 55 μL/60 mg for aniline. After each cycles, the loaded **COP** powder (stationary phase) was washed very well with water, ethyl acetate and methanol to remove the adsorbed solvent (aniline) from the pores of **COP**. After that the used **COP** was dried below 90 °C and used for the next cycle. The **COP** was reused and the **COP** retained its activity after five cycles (Fig. S14, ESI†). For the purpose of extraction of aniline from the aniline/water mixture, we have directly used the resultant **COP** powder. The adsorption mechanism was followed to extract aniline where **COP** acts as an adsorbent for aniline in aqueous solution. Here, 45 mg of **COP** powder was added to a 3 mL aqueous solution of aniline with a concentration of 222 mg L^{-1} and allowed to stir at 25 °C. The UV-Vis spectra of the resultant solution were recorded at different time intervals. The gradual decrease in aniline absorbance suggests quick adsorption performance (Fig. S15a, ESI†). The **COP** exhibits significant adsorption performance for aniline, removing 83.5% of aniline in 8 h and achieves adsorption equilibrium (using eqn S1, ESI†). The removal rate of **COP** for aniline is substantially higher, implying that the $-NH_2$ group of aniline plays a crucial role in the adsorption process towards **COP** functionalities. Compared with nitrobenzene, **COP** is a better adsorbent material with fast adsorption for aniline, which is due to the well-defined porous structure and surface functionalities. The adsorption process demonstrates that the incorporated hydrazide groups of **COP** are favourable for adsorption due to possible H-bonding and acid–base interactions.

Conclusions

In summary, we synthesized a covalent organic polymer (**COP**) *via* dynamic covalent gel (DCG) through imine bond formation. *N*,*N*-Dimethyl acetamide played a significant role in the scalable synthesis of **COP** *via* gel formation. The emissive gel served as an interesting protocol for the construction of porous **COP**. The green emission of **COP-gel** was caused by an aggregation-induced emission (AIE) phenomenon, which was assisted by H-bonding and several non-covalent interactions. On the other hand, the disperse solution of **COP** in DMA showed bluish-white light emission. The degree of aggregation was important in determining the emission colour of **COP** in gel and solution states. The dried **COP** had the ability to easily adsorb aniline molecules into its cavities and separate them from binary mixtures of aniline/nitrobenzene and aniline/water. Our findings represent a significant advancement in the development of functionalized **COP** with excellent scalability under ambient conditions, as well as significant physical insights into the separation of aniline from miscible binary solvent mixtures.

Conflicts of interest

There are no conflicts to declare.

Acknowledgements

The authors gratefully acknowledge CSIR, Government of India (Project No. 01(2936)/18/EMR-II), for financial support and SIC, IIT Indore, for providing the required instrumental facilities. SM thanks IIT Indore, TG acknowledges DST Inspire Fellowship, Government of India, and AS acknowledges CSIR, Government of India, for their doctoral fellowship.

Notes and references

1 P. Puthiaraj, Y.-R. Lee, S. Zhang and W.-S. Ahn, *J. Mater. Chem. A*, 2016, **4**, 16288–16311.
2 V. S. Vyas, F. Haase, L. Stegbauer, G. Savasci, F. Podjaski, C. Ochsenfeld and B. V. Lotsch, *Nat. Commun.*, 2015, **6**, 8508.
3 P. Wang, F. Zhou, C. Zhang, S.-Y. Yin, L. Teng, L. Chen, X.-X. Hu, H. W. Liu, X. Yin and X.-B. Zhang, *Chem. Sci.*, 2018, **9**, 8402–8408.
4 Z. Miao, G. Liu, Y. Cui, Z. Liu, J. Li, F. Han, Y. Liu, X. Sun, X. Gong, Y. Zhai, Y. Zhao and Y. Zeng, *Angew. Chem., Int. Ed.*, 2019, **58**, 4906–4910.
5 C. Qian, Q.-Y. Qi, G.-F. Jiang, F.-Z. Cui, Y. Tian and X. Zhao, *J. Am. Chem. Soc.*, 2017, **139**, 6736–6743.
6 W. Luo, Y. Zhu, J. Zhang, J. He, Z. Chi, P. W. Miller, L. Chen and C.-Y. Su, *Chem. Commun.*, 2014, **50**, 11942–11945.
7 H. Zhong, Y. Gong, W. Liu, B. Zhang, S. Hu and R. Wang, *Dalton Trans.*, 2019, **48**, 2345–2351.
8 P. Song, Z. Zhang, L. Yu, P. Wang, Q. Wang and Y. Chen, *New. J. Chem.*, 2020, **44**, 8572–8577.
9 B. Mondal, D. Bairagi, N. Nandi, B. Hansda, K. S. Das, C. J. C. Edwards-Gayle, V. Castelletto, I. W. Hamley and A. Banerjee, *Langmuir*, 2020, **36**, 12942–12953.
10 S. K. Nandi, S. Kumar, S. Roy Chowdhury, I.-O. J. Ibukun and D. Haldar, *ChemistrySelect*, 2021, **6**, 4448–4455.
11 S. Das, P. Heasman, T. Ben and S. Qiu, *Chem. Rev.*, 2017, **117**, 1515–1563.
12 L. Tan and B. Tan, *Chem. Soc. Rev.*, 2017, **46**, 3322–3356.
13 X. Li, L. Jin, L. Huang, X. Ge, H. Deng, H. Wang, Y. Li, L. Chai and S. Ma, *J. Environ. Chem. Eng.*, 2021, **9**, 106357.
14 P. Samanta, A. V. Desai, S. Let and S. K. Ghosh, *ACS Sustainable Chem. Eng.*, 2019, **7**, 7456–7478.
15 K. Dey, S. H. Kunjattu, A. M. Chahande and R. Banerjee, *Angew. Chem., Int. Ed.*, 2020, **59**, 1161–1165.
16 W. Wang, M. Zhou and D. Yuan, *J. Mater. Chem. A*, 2017, **5**, 1334–1347.
17 Q. Chen, M. Luo, P. Hammershøj, D. Zhou, Y. Han, B. W. Laursen, C.-G. Yan and B.-H. Han, *J. Am. Chem. Soc.*, 2012, **134**, 6084–6087.
18 Y. Yuan, F. Sun, L. Li, P. Cui and G. Zhu, *Nat. Commun.*, 2014, **5**, 4260.
19 G. He, R. Zhang and Z. Jiang, *Acc. Mater. Res.*, 2021, **2**, 630–643.
20 S. Yuan, X. Li, J. Zhu, G. Zhang, P. V. Puyvelde and B. V. Bruggen, *Chem. Soc. Rev.*, 2019, **48**, 2665–2681.

21 S. Zhang, S. Zhao, X. Jing, Z. Niu and X. Feng, *Org. Chem. Front.*, 2021, **8**, 3943–3967.
22 J. Liu, G. Han, D. Zhao, K. Lu, J. Gao and T.-S. Chung, *Sci. Adv.*, 2020, **6**, 1110.
23 M. Ulbricht, *Curr. Opin. Chem. Eng.*, 2020, **28**, 60–65.
24 D.-W. Gao, Q. Hu, H. Pan, J. Jiang and P. Wang, *Bioresour. Technol.*, 2015, **193**, 507–512.
25 F. An, X. Feng and B. Gao, *J. Hazard. Mater.*, 2010, **178**, 499–504.
26 K. Yang, W. Wu, Q. Jing and L. Zhu, *Environ. Sci. Technol.*, 2008, **42**, 7931–7936.
27 Y. Zhou, X. Gu, R. Zhang and J. Lu, *Ind. Eng. Chem. Res.*, 2014, **53**, 887–894.
28 Y. Chen, B. Wang, X. Wang, L.-H. Xie, J. Li, Y. Xie and J.-R. Li, *ACS Appl. Mater. Interfaces*, 2017, **9**, 27027–27035.
29 S. H. Gheewala and A. P. Annachhatre, *Water Sci. Technol.*, 1997, **36**, 53–58.
30 P. G. Jessop, L. Phan, A. Carrier, S. Robinson, C. J. Durr and J. R. Harjani, *Green Chem.*, 2010, **12**, 809–814.
31 P. G. Jessop, S. M. Mercer and D. J. Heldebrant, *Energy Environ. Sci.*, 2012, **5**, 7240–7253.
32 W. Li, B. Xu, Z. Lei and C. Dai, *Chem. Eng. Process.*, 2018, **126**, 81–89.
33 J. Gu, X. You, C. Tao, J. Li, W. Shen and J. Li, *Chem. Eng. Res. Des.*, 2018, **133**, 303–313.
34 W. Ma, J. Sun, W. Hongpu and R. Wang, *Ind. Eng. Chem.*, 2010, **39**, 781–782.
35 S. Maiti, B. Mandal, M. Sharma, S. Mukherjee and A. K. Das, *Chem. Commun.*, 2020, **56**, 9348–9351.
36 F. J. U.-Romo, C. J. Doonan, H. Furukawa, K. Oisaki and O. M. Yaghi, *J. Am. Chem. Soc.*, 2011, **133**, 11478–11481.
37 S. Maiti, A. Roy Chowdhury and A. K. Das, *ChemNanoMat*, 2019, **6**, 99–106.
38 A. Roy Chowdhury, S. Maiti, A. Mondal and A. K. Das, *J. Phys. Chem. C*, 2020, **124**, 7835–7843.
39 S. Dalapati, E. Jin, M. Addicoat, T. Heine and D. Jiang, *J. Am. Chem. Soc.*, 2016, **138**, 5797–5800.
40 D. Wang, S.-M. Li, Y.-F. Li, X.-J. Zheng and L.-P. Jin, *Dalton Trans.*, 2016, **45**, 8316–8319.
41 H.-Q. Yin, F. Yin and X.-B. Yin, *Chem. Sci.*, 2019, **10**, 11103–11109.
42 S. Riebe, C. Vallet, F. V. Vight, D. G. Abradelo, C. Wölper, P.-D. C. A. Strassert, G. Jansen, S. Knauer and J. Voskuhl, *Chem. – Eur. J.*, 2017, **23**, 13660–13668.
43 F.-Z. Cui, J.-J. Xie, S.-Y. Jiang, S.-X. Gan, D.-L. Ma, R.-R. Liang, G.-F. Jiang and X. Zhao, *Chem. Commun.*, 2019, **55**, 4550–4553.
44 S. Feng, S. Gong and G. Feng, *Chem. Commun.*, 2020, **56**, 2511–2513.
45 Y. Liu, Z. Qiu, H. Zhong, X. Zhao, W. Huang and X. Xing, *RSC Adv.*, 2020, **10**, 12953–12961.
46 S. Ravi, P. Puthiaraj, K. Yu and W.-S. Ahn, *ACS Appl. Mater. Interfaces*, 2019, **11**, 11488–11497.
47 L. Deng, X. Kang, T. Quan, L. Yang, S. Liu, K. Zhang, M. Gao, Z. Xia and D. Gao, *ACS Appl. Mater. Interfaces*, 2021, **13**, 33449–33463.
48 J.-X. Zhou, X.-S. Luo, X. Liu, Y. Qiao, P. Wang, D. Mecerreyes, N. Bogliotti, S.-L. Chen and M.-H. Huang, *J. Mater. Chem. A*, 2018, **6**, 5608–5612.
49 Y. Liu, X. Fan, X. Jia, B. Zhang, H. Zhang, A. Zhang and Q. Zhang, *J. Mater. Sci.*, 2016, **51**, 8579–8592.
50 A. R. A. Hamid, R. Mhanna, R. Lefort, A. Ghoufi, C. Alba-Simionesco, B. Frick and D. Morineau, *J. Phys. Chem. C*, 2016, **120**, 9245–9252.
51 C. A. Hunter, *J. Mol. Biol.*, 1993, **230**, 1025–1054.